THE WATER VAPOR SPECTRUM OF APM 08279+5255: X-RAY HEATING AND INFRARED PUMPING OVER HUNDREDS OF PARSECS

C.M. Bradford[1,2], A.D. Bolatto[3], P.R. Maloney[4], J.E. Aguirre[4,5], J.J. Bock[1,2], J. Glenn[4], J. Kamenetzky[4], R. Lupu[5], H. Matsuhara[7], E.J. Murphy[7], B.J. Naylor[2,1], H.T. Nguyen[1], K. Scott[5], J. Zmuidzinas[2,1]

Accepted for Publication in the Astrophysical Journal Letters

ABSTRACT

We present the rest-frame 200–320 μm spectrum of the z=3.91 quasar APM 08279+5255, obtained with Z-Spec at the Caltech Submillimeter Observatory. In addition to the $J = 8 \to 7$ to $J = 13 \to 12$ CO rotational transitions which dominate the CO cooling, we find six transitions of water originating at energy levels ranging up to 643 K. Most are first detections at high redshift, and we have confirmed one transition with CARMA. The CO cooling is well-described by our XDR model, assuming $L_{1-100\,\mathrm{keV}} \sim 1 \times 10^{46}\,\mathrm{erg\,s^{-1}}$, and that the gas is distributed over a 550-pc sizescale, per the now-favored $\mu=4$ lensing model. The total observed cooling in water corresponds to 6.5×10^9 $L_\odot$, comparable to that of CO. We compare the water spectrum with that of Mrk 231, finding that the intensity ratios among the high-lying lines are similar, but with a total luminosity scaled up by a factor of $\sim$50. Using this scaling, we estimate an average water abundance relative to H_2 of 1.4×10^{-7}, a good match to the prediction of the chemical network in the XDR model. As with Mrk 231, the high-lying water transitions are excited radiatively via absorption in the rest-frame far-infrared, and we show that the powerful dust continuum in APM 08279+5255 is more than sufficient to pump this massive reservoir of warm water vapor.

Subject headings: galaxies: active — quasars: emission lines — ISM: molecules — instrumentation: spectrographs

1. INTRODUCTION

1.1. *Water as a Molecular Gas Coolant and Radiation Field Probe*

Though virtually impossible to observe in the local Universe from the ground, H_2O is an important constituent of interstellar gas under the right conditions. The species is chemically enhanced for temperatures above a few hundred Kelvin (Draine & Roberge 1982), and is sublimated from grain mantles as dust is heated to $\sim$100 K. In these conditions, it becomes an important gas-phase repository for oxygen, with abundance approaching that of CO (e.g. Cernicharo et al. (2006)). With water's large dipole moment, the network of rotational transitions can either be a dominant molecular coolant (for $T > 300\,\mathrm{K}$ and $n_{H_2} > 10^5 \mathrm{cm}^{-3}$; Hollenbach & McKee (1979); Neufeld & Melnick (1987); Neufeld & Kaufman (1993, and references therein)), or a pathway for coupling mid- and far-infrared continuum radiation into the gas if the local continuum is sufficiently strong (e.g. Scoville & Kwan (1976).

Many of the most important H_2O transitions lie in the short submillimeter, between 200–300 μm, which has until recently been inaccessible in the local universe, and has been only sparsely explored at high redshifts via observations in the millimeter band. With the advent of broadband spectrometers enabled by high-performance bolometer arrays (Herschel SPIRE–Griffin et al. (2010) and Z-Spec–e.g. Earle et al. (2006)), the water spectrum can be explored on galaxy scales locally and at high redshift. Water is not an important coolant in the overall energy budget of the gas in the Milky Way (via COBE, Fixsen et al. (1999)) or even in the nucleus of the nearby starburst galaxy M82 (Panuzzo et al. 2010). However, in extreme ULIRGs such as Arp 220 (Rangwala et al. 2011), and Mrk 231 (van der Werf et al. (2010, hereafter vdW10), González-Alfonso et al. (2010, hereafter GA10)), the most luminous H_2O transitions lines can be comparable in strength to those of CO.

Through comparison with water excitation models, GA10 show that the water emission lines in Mrk 231 measured with SPIRE are not produced by purely collisional excitation; the ratio of high-level transitions to the lower-level and ground-state transitions is too large, even for shock-like conditions. They present a model in which the 200–300 μm water emission spectrum is pumped by the absorption of shorter-wavelength continuum photons, a scenario supported by absorption measurements with the ISO LWS (González-Alfonso et al. 2008). The excitation of water is thus coupled closely to the dust continuum intensity, and GA10 are able to use the ISO + SPIRE lines to constrain the size and opacity of the dust continuum source in Mrk 231 between 30 and 150 microns, concluding that it is $\sim$110–180 pc in size.

We might expect to find similar processes at work in the early Universe, and our wideband 1 mm surveys with Z-Spec are revealing H_2O in a handful of high-redshift objects (Bradford et al.; 2009 (hereafter B09), Lupu et al. 2010; Omont et al. 2011). We present here a study of APM 08279+5255 at z=3.91, a particularly

[1] Jet Propulsion Laboratory, California Institute of Technology, Pasadena, CA, 91109, USA
[2] California Institute of Technology, Pasadena, CA, 91125, USA
[3] University of Maryland, College Park, MD, 20742-2421, USA
[4] University of Colorado, Boulder, CO, 80303, USA
[5] University of Pennsylvania, Philadelphia, PA, 19104, USA
[6] Institute for Space and Astronautical Science, Japan Aerospace and Exploration Agency, Sagamihara, Japan
[7] Observatories of the Carnegie Institution for Science, 813 Santa Barbara Street, Pasadena, CA 91101, USA

convenient redshift for characterizing the water emission spectrum in the 1 mm band.

1.2. *APM 08279+5255*

APM 08279+5255 is an unusual source by any measure. It exhibits an apparent total bolometric luminosity of 7×10^{15} $L_{\odot}$, dominated by warm AGN-heated dust peaking in the rest-frame 15–30 μm regime (Riechers et al. 2009, and references therein, hereafter R09). There is a cold dust component identified in the rest-frame far-IR and submillimeter which contributes $\sim$3% of the total energy. This may be produced by star formation, and the [OIII] 88 μm luminosity ($1.06 \times 10^{11}/\mu$ $L_{\odot}$) is consistent with star formation contributing up to $\sim$35% of this far-IR luminosity (Ferkinhoff et al. 2010), or $\sim$1% of the total in the system. APM 08279+5255 has been studied in detail with interferometric observations of CO ranging from $J=1\to0$ and $J=2\to1$ with the VLA (Papadopoulos et al. (2001), more recently R09) to $J=11\to10$ with the Plateau de Bure Interferometer (PdB) (Weiß et al. 2007, hereafter W07). The compact CO morphology (at least at $J=1\to0$) is similar to the image of the optical quasar—only just marginally resolved into sub-images at $0.4''$, and R09 model the CO $J=1\to0$-emitting gas as a R$\sim$550 pc disk, magnified by $\mu=4$. We adopt this magnification factor, and a luminosity distance of 35,565 Mpc (appropriate for $H_0 = 71$, $\Omega_M = 0.27$, $\Omega_\Lambda = 0.73$). The W07 CO measurements then translate to an intrinsic molecular gas mass of $M_{\text{total}} \sim 1.0 \times 10^{11}$ $M_{\odot}$ using an adopted scale factor of 5.3×10^{11} $M_{\odot}$ (K km s^{-1} pc^2)$^{-1}$.

In the R09 lensing model, the magnification is not sharply peaked in the central few hundred parsecs: $\mu(R)$ ranges from 3–5 out to source radius $R \sim$10 kpc. If this is correct, then the CO line ratios and the gas conditions inferred from CO (W07) are largely independent of the lensing, and the high-J CO emission in APM 08279+5255 is particularly unusual among extragalactic sources. To reproduce the ratios among the low-J and high-J CO transitions, W07 require at least two components with conditions ranging from cool and dense (T$\sim$65 K, n$_{\text{H}_2}\sim1\times10^5$ cm^{-3}) to warmer and less dense (T$\sim$225 K, n$_{\text{H}_2}\sim1\times10^4$ cm^{-3}).

2. OBSERVATIONS

APM 08279+5255 was observed with Z-Spec at the Caltech Submillimeter Observatory (CSO) on a total of 13 nights among 4 observing campaigns: 2008 March 23–28, 2008 April 4–16, 2009 January 6–9 and 2009 February 23–27. We used the chop-and-node mode with a 20 second nod period and a 1.6 Hz, $90''$ chop. The total integration time (including chopping) is 25.3 hours, with a range of telluric water vapor burdens; $\tau_{225\text{GHz}}$ ranged from 0.04 to 0.20, with a median of 0.083 and a mean of 0.102. With all data incorporated in a weighted coaddition, the sensitivity referred to the total integration time ranges from 750 mJy s$^{1/2}$ in the middle of the band (producing a 2.5 mJy channel RMS) to 1100 mJy sec$^{1/2}$ at the band edges (3.6 mJy channel RMS), with greater degradation below 200 GHz. The data are calibrated using Mars and Uranus, with quasars as secondary calibrators using the method described in B09. Figure 1 shows the spectrum and the line fits described below.

2.1. *CARMA Follow-Up*

The source was also observed using the 15-element Combined Array for Research in Millimeter-wave Astronomy (CARMA, (Bock et al. 2006)), (Figure 2). On 2009 November 9 and 15, with the array in its C configuration. The upper sideband was tuned to $\nu_{USB} = 236.75$ GHz, corresponding to the H$_2$O $3_{2,1} \to 3_{1,2}$ transition at $z = 3.9119$, the redshift measured with PdB for CO $J=9\to8$ (the highest-J transition measured with the PdB) (W07). The lower sideband was centered on $\nu_{LSB} = 231.14$ GHz. The correlator was configured in its 3×468.75 MHz setting with partially overlapping windows, yielding an effective coverage of $\Delta\nu \approx 1.3$ GHz ($\Delta v \approx 1600$ km s^{-1}) with a native resolution of ≈ 31.25 MHz (≈ 39.6 km s^{-1}).

The double sideband system temperature was T$_{sys} \sim 280 - 480$ K, and the total integration time was 9 hours. The quasar $0359 + 509$ was the astronomical bandpass calibrator ($S_\nu \sim 3.5$ Jy), and Mars was the absolute flux calibrator. The quasars $0927 + 390$ ($S_\nu \sim 2.3$ Jy) and $0920 + 446$ ($S_\nu \sim 1.0$ Jy) were primary and secondary phase calibrators, respectively, on a calibration cycle of 10 minutes. The phase RMS on $0927 + 390$ after self calibration was approximately $25°$. Atmospheric decorrelation effects were estimated to be 35%, and the fluxes have been corrected accordingly. This is not unexpected since the observations were obtained in a mid-size configuration, with typical baselines of ~ 360 m.

The synthesized beam size is $\theta = 0.80'' \times 0.64''$ with $PA = -70°4$. Fitting to the LSB and the USB images are very consistent and suggest that APM 08279+5255 is slightly resolved with an intrinsic angular size of $\theta \approx 0.4''$, in agreement with other observations of the source angular size (Krips et al. 2007).

3. RESULTS, CONTINUUM AND LINE FLUX EXTRACTIONS

A model spectrum consisting of a a power-law continuum with 15 Gaussian spectral lines is fit to the 160 bolometer flux values, incorporating their measured spectral response profiles using the method described in Naylor et al. (2010). The redshift is fixed at 3.9119, and the line width is $\Delta v_{\text{FWHM}} = 550$ km s^{-1}. This width is greater than that reported by W07 for the low-J transitions, but is consistent with values measured for the $J=9\to8$ $J=10\to9$ CO transitions. In any case, our fits to the Z-Spec spectrum are not very sensitive to the adopted line width. The fitted fluxes and resulting uncertainties are presented in Table 1.

Our CO fluxes are consistent with the W07 IRAM measurements to within the uncertainties, though we do find systematically larger values, e.g. for $J=9\to8$ and $J=11\to10$ (35–45%). Since the continuum measurements are consistent to better than this (see Figure 1) we rule out global calibration problems at this level. It may be that Z-Spec is coupling flux in high-velocity wings of the lines which would be missed in the IRAM spectra, or there could be spatially extended CO emission that the interferometer resolves out. Given the coarse resolution, it is also possible that other transitions near CO are contaminating the Z-Spec fitted flux, though aside from the $J=10\to9$ transition, there are no significant candidates in the SPIRE Mrk 231 spectrum
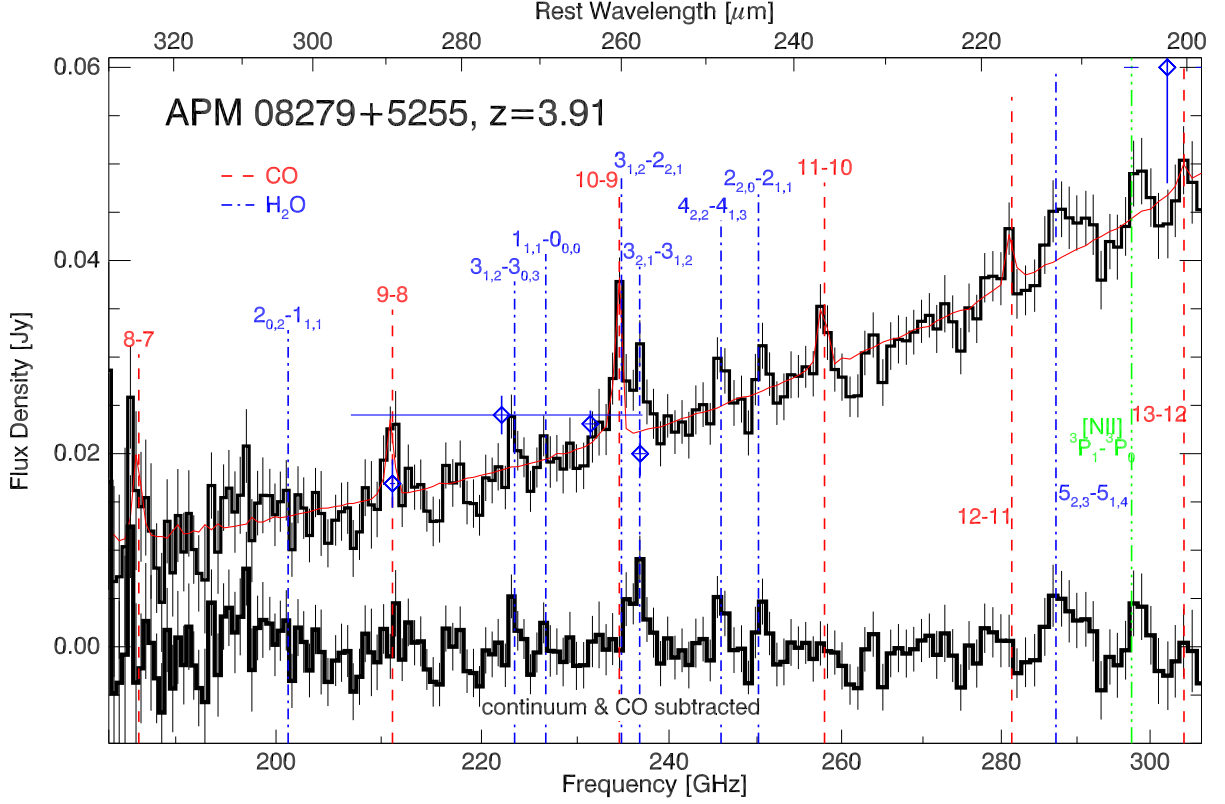
FIG. 1.— Z-Spec spectrum of APM 08279+5255. Dashed vertical lines show all transitions of CO and H$_2$O with upper-level energies below 700 K which lie in the band. The position of the [NII] 205 μm transition is also noted. Diamonds show continuum measurements from (in increasing frequency): Plateau de Bure (W07), SCUBA (Lewis et al. 1998), CARMA (this work), CARMA (this work), and the SMA (average of two sidebands—horizontal and vertical bars indicate bandwidth and uncertainty) (Krips et al. 2007). The lower spectrum shows the data with a fit to the continuum and CO lines subtracted.
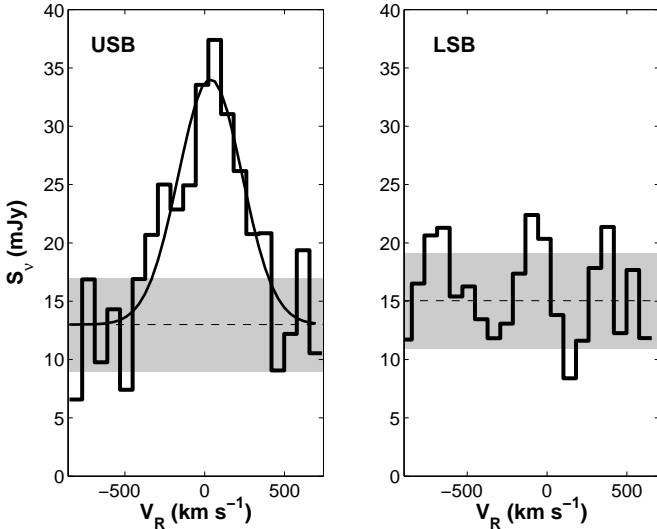

FIG. 2.— CARMA spectrum of the $3_{2,1} \rightarrow 3_{1,2}$ H$_2$O transition. The velocity scales refers to $z = 3.9119$. The plotted spectra are not corrected for the atmospheric decorrelation, though the entries in Table 1 are.

(van der Werf et al. 2010). In any case, our CARMA measurement is consistent with Z-Spec in both the line flux and continuum to better than the statistical uncertainties.

CO $J = 10 \rightarrow 9$ is clearly blended with the H$_2$O $3_{1,2} \rightarrow 2_{2,1}$ transition; the two transitions are separated by 297 km s^{-1}, about 1/3 of a Z-Spec channel. We fit the two simultaneously, but only their sum is meaningful. We estimate the flux of CO $J = 10 \rightarrow 9$ as the geometric mean of the $J = 9 \rightarrow 8$ and $J = 11 \rightarrow 10$ intensities in temperature units, and then subtract this value from the fitted flux of the CO+water blend to arrive at an estimate of the flux for the water line. We find that the water and CO fluxes are comparable, though the formal SNR for each is modest (~ 2.0) as the errors are propagated in this estimate.

Figure 1 and Table 1 show all eight H$_2$O transitions in the band with upper level energies less than 700 K. Of these, we detect four in emission with $>2.3\sigma$ significance. While less than the customary 3σ, 2.3σ corresponds to a likelihood of only $(1 - erf(SNR/\sqrt{2}))/2 = 1.0\%$ that the transition is not real with positive flux, if the noise is Gaussian. In addition to $3_{1,2} \rightarrow 2_{2,1}$ described above (2σ is only 2.2% likely to be false), we tentatively identify two additional transitions in emission at lower significance ($1_{1,1} \rightarrow 0_{0,0}$ and $2_{2,0} \rightarrow 2_{1,1}$) and estimate fluxes and upper limits. $2_{0,2} \rightarrow 1_{1,1}$ can only offer an upper limit. In Figure 3, we plot 2σ upper limits, corresponding to a 98% confidence level.

The ground-state fine-structure transition of [NII] ($^3P_1 \rightarrow {}^3P_0$, λ_{rest}=205.18 μm) is identified as tentatively in emission at low significance (1.4σ). The value is consistent with the lower limit obtained by Krips et al. (2007) with the SMA ($3\sigma < 9$ Jy km s^{-1} in a single beam beam, $3\sigma < 16$ Jy km s^{-1} if scaled to the continuum source size (Ferkinhoff et al. 2010)).

TABLE 1
1-mm Line Intensity Measurements in APM 08279+5255

transition	E_{upper} [K]	ν_{rest} [GHz]	ν_{obs} [GHz]	flux [Jy km/s]	1σ err [Jy km/s][a]	$L_{intrinsic}$ [10^8 L$_\odot$][b]
CO $J=8\rightarrow7$	199	921.80	187.7	12.1	8.3	7.4 ± 5.1
CO $J=9\rightarrow8$	249	1036.91	211.1	16.0	3.8	11.0 ± 2.6
IRAM 30-m (W07)				11.1	2.2	7.7 ± 1.5
IRAM Plateau de Bure (W07)				12.5	2.4	8.6 ± 1.7
CO $J=10\rightarrow9$	304	1151.99	234.6	15.2[c]	7.2	11.6 ± 5.5
IRAM 30-m (W07)				11.9	2.4	9.1 ± 1.8
CO $J=11\rightarrow10$	365	1267.02	258.0	14.4	4.5	12.1 ± 3.8
IRAM 30-m (W07)				10.4	2.1	9.2 ± 1.8
CO $J=12\rightarrow11$	431	1381.00	281.4	9.5	5.0	8.8 ± 4.6
CO $J=13\rightarrow12$	503	1496.92	304.8	4.4	6.1	
H_2O $2_{0,2}\rightarrow1_{1,1}$	101	987.93	201.2	1.9	4.1	<8.1 (3σ)
H_2O $3_{1,2}\rightarrow3_{0,3}$	250	1097.40	223.5	8.1	3.5	5.9 ± 2.6
H_2O $1_{1,1}\rightarrow0_{0,0}$	53.4	1113.34	226.7	4.6	3.7	3.4 ± 2.7 $(3\sigma<8.2)$
H_2O $3_{1,2}\rightarrow2_{2,1}$	250	1153.13	234.8	14.5[c]	7.2	11.1 ± 5.5
H_2O $3_{2,1}\rightarrow3_{1,2}$	305	1162.91	236.8	16.0	3.5	12.4 ± 3.0
CARMA (this work)				16.3	3.5	12.6 ± 2.7
H_2O $4_{2,2}\rightarrow4_{1,3}$	455	1207.64	245.9	12.8	4.3	10.3 ± 4.1
H_2O $2_{2,0}\rightarrow2_{1,1}$	196	1228.79	250.2	7.9	4.4	6.4 ± 4.0 $(3\sigma<12.0)$
H_2O $5_{2,3}\rightarrow5_{1,4}$	643	1410.62	287.2	16.0	6.3	15.0 ± 5.2
NII $^3P_1\rightarrow^3P_0$	70.1	1461.0	297.4	7.6	5.4	7.4 ± 5.1

[a] Z-Spec fluxes include statistical uncertainties only, IRAM uncertainties are $\pm20\%$, per W07.
[b] All luminosities are corrected for lensing, assuming a magnification factor of 4.
[c] CO $J=10\rightarrow9$ and H_2O $3_{1,2}\rightarrow2_{2,1}$ are blended, see discussion in text.

4. ANALYSIS AND DISCUSSION

4.1. *CO Emission and XDR heating*

We find that the ratios among the high-J CO transitions are consistent with the excitation model presented in W07. If the IRAM fluxes are increased to match the Z-Spec values with the factor of 1.4 described above, our $J=8\rightarrow7$ and $J=12\rightarrow11$ fluxes and the $J=13\rightarrow12$ limit all fall on the CO excitation curves in Figures 7 and 9 of W07, matching to well within the statistical uncertainties. We estimate a total lensing-corrected CO luminosity of $\sim7\times10^9$ L$_\odot$, a fraction 1.4×10^{-4} of the 5×10^{13} L$_\odot$ output in the far-IR per the decomposition of R09. This total CO luminosity fraction is not unusually high; it is comparable to the value in local starburst galaxies and ULIRGs for which the spectra have now been measured with Herschel SPIRE. L_{CO}/L_{IR} is 1.25×10^{-4} in M82 (Panuzzo et al. 2010), 1.0×10^{-4} in Arp 220 (Rangwala et al. 2011), and 7×10^{-5} in Mrk 231 (vdW10). However, as W07 have noted, the CO excitation of APM 08279+5255 is much higher: the $J=11\rightarrow10$ to $J=6\rightarrow5$ luminosity ratio, for example ranges from 0.54 ± 0.13 in M82 to ~ 1 in Mrk 231 to 2.5–3.5 in APM 08279+5255, depending on the calibration. Since the high-lying CO transitions in Mrk 231 cannot be understood in a reasonable PDR framework, the even more extreme ratios in APM 08279+5255 cannot be fit by PDR models either.

Given the powerful hard X-ray source, it is likely the high-J CO emission is due to gas cooling in X-ray dominated regions (XDRs, Maloney et al. (1996)), as has been modeled for both the Mrk 231 and the Cloverleaf system (B09). For APM 08279+5255, we estimate an intrinsic 1–100 keV luminosity of 1×10^{46} erg s^{-1}, by extrapolating the apparent luminosity in the rest-frame 2–10 keV range of 2.3×10^{46} erg s^{-1} per Just et al. (2007). This is similar to the hard X-ray luminosity inferred for the Cloverleaf, and if we assume the same attenuating column of $N_{H,att} = 3 \times 10^{23}$ cm^{-3} (as is required to maintain a molecular phase), then we can use the same model as in B09 to consider the CO excitation (Figures 6, 7, 8 in B09). Assuming the CO emission emerges from a 550-pc disk as per R09, then the CO surface brightness (erg s^{-1} cm^{-2}) in APM 08279+5255 is 0.7–0.8 erg s^{-1} cm^{-2}, some 3.5–4 times that of the Cloverleaf. This emergent flux is readily produced with R<650 pc and $n_H>2\times10^5$ cm^{-3} ($n_{H_2}>1\times10^5$ cm^{-3} if fully molecular). While the required density is on the high end of that inferred in the W07 CO analysis; this is overall a good match to the observed parameters.

4.2. *Water Emission and Radiative Pumping.*

Totaling the available transitions in our band, we find a total luminosity of 6.5×10^9 L$_\odot$ in the water rotational network. This is a lower bound, but is already close to the total CO emission, suggesting that water is energetically important to the gas. As GA10 found for Mrk 231, the ratio of luminosity in the high-excitation transitions relative to the low-lying ones indicates that the high-excitation levels are not excited collisionally. The conditions inferred by W07 using CO (temperature from 70–200 K and n_{H_2} between 10^4 and 10^5 cm^{-3}) are well below even the extreme conditions considered by GA10 (T=200 K, $n_{H_2}=1.5\times10^6$ cm^{-3}) in considering collisional excitation.

Figure 3 shows a comparison of the APM 08279+5255 H_2O spectrum to that of Mrk 231 (adopting d_L=184 Mpc). To our measurement accuracy, the emission in the high-lying lines in APM 08279+5255 resembles that in Mrk 231, scaled up by $\sim50\times$. In fact, APM 08279+5255 shows an even higher ratio of the $E_{upper} > 200$ K transitions to the lower-energy ones. There is plenty of molecular material in the source—the R09 molecular gas mass estimate is a factor

of 22 times the GA10 estimate for Mrk 231, including all 3 components, but it is some $300\times$ the modeled warm component which dominates the high-lying water emission in Mrk 231. Thus even modest water abundance throughout, or an abundance similar to that obtained in Mrk 231 in 1/6 of the total gas reservoir would be sufficient to produce the observed luminosity in APM 08279+5255, if it is suitably excited.

The low significance of the detections and lack of higher-frequency coverage for the absorption transitions does not warrant a detailed radiative transfer model, but it is easy to show that the powerful dust continuum in APM 08279+5255 can readily pump the observed water transitions with the same mechanism as that modeled by GA10 for Mrk 231. Assuming spherical symmetry, the observed flux constrains the size of a fiducial region R_s around a dust emitting source via:

$$(\nu F_\nu)_{obs}\, \mu^{-1} = \frac{(\nu L_\nu)_{em}}{4\pi d_L^2} = \frac{R_s^2}{d_L^2}\,\nu_{em}\int I_{\nu\, em}\, d\Omega \quad (1)$$

where d_L is the luminosity distance, and μ is the magnification factor. $I_\nu(\Omega)$ is the specific intensity produced by the dust distribution; it captures brightness temperature and opacity as a function of viewing angle. For a pumping transition at ν_{em} this integral of I_ν over solid angle is the quantity that sets the pumping rate per molecule in a given transition. Holding this constant allows an estimate of the ratio of the size scale over which similar pump conditions exist in APM 08279+5255 as those in Mrk 231, through the scaling:

$$R_s \propto d_L \left[(\nu F_\nu)_{obs}\, \mu^{-1}\right]^{1/2}, \quad (2)$$

giving

$$V_w \propto R_s^3 \propto d_L^3 \left[(\nu F_\nu)_{obs}\, \mu^{-1}\right]^{3/2} \quad (3)$$

As an example we consider pumping of the $3_{1,3}$ level with absorption at 58μm, producing the $4_{2,2}\rightarrow4_{1,3}$ transition in emission. Given the observed fluxes, the scaling above suggests that R_s is 5.1 times larger for APM 08279+5255 than for Mrk 231. For similar geometries, then, the continuum-emitting source in APM 08279+5255 is capable of illuminating a volume $\sim R_s^3 \sim 130$ times larger than Mrk 231 with a similar pump rate. This is a reasonable match to the factor of 50–90 larger luminosity in this transition in APM 08279+5255. We expect that for APM 08279+5255, the higher color temperature would preferentially pump via higher-frequency far-IR transitions relative to Mrk 231, and this likely explains the increased flux in the $5_{2,3}\rightarrow5_{1,4}$ transition (pumped via 45 μm) and the reduced flux in $3_{1,2}\rightarrow2_{2,1}$ (pumped via 75 μm).

The Mrk 231 warm water-emitting component is modeled by GA10 as a sphere of dust and gas of size 110–180 pc. With the above scaling, we know that that similar pump conditions must exist in APM 08279+5255 out to distances of 560–920 pc. This may seem extreme, but APM 08279+5255 is an extremely powerful system; consider that the smallest possible physical size for the 220 K source is in the limit of an optically-thick (at $\lambda_{\rm peak}$) sphere, for which $R_{min}\sim215$ pc. Thus if the molecular gas is really situated in a R$\sim$550-pc disk per the model of R09, then a large fraction of the molecular mass in this system is capable of being pumped to the level of
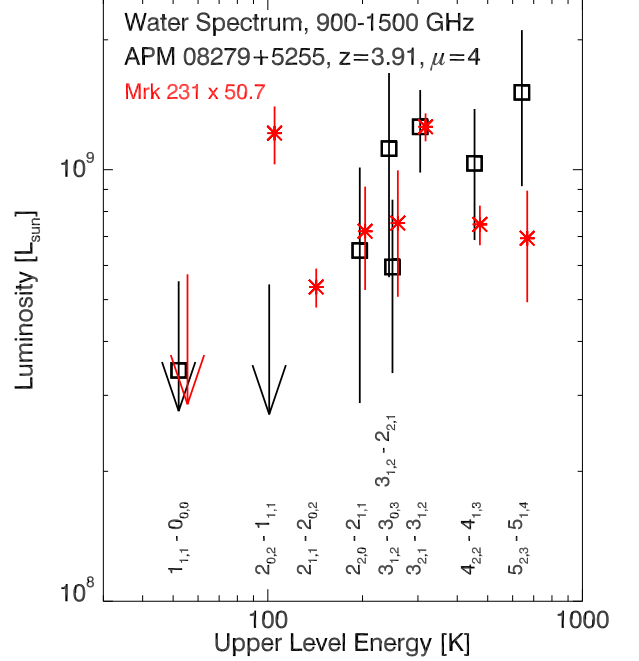

FIG. 3.— Comparison of the water spectrum in Mrk 231 with that in APM 08279+5255, as measured with Z-Spec. Downward arrows show limits at 2σ. The H_2O $3_{1,2}\rightarrow2_{2,1}$ flux is not measured in Mrk 231, though as vdW10 note, the $J{=}10\rightarrow9$ transition likely includes flux from this line.

the warm component in the Mrk 231 model. Indeed, the simple model suggests that the water must exist at such large distances because the system is so opaque. If we require that the same 220 K, 215-pc dust component account for the emission at $\lambda_{\rm rest}{=}250$ μm, then it must have an opacity of $\sim$0.8 at this wavelength. Any contribution from lower-temperature material requires a combination of larger opacity and/or larger physical size. In the spherically-symmetric model then, this indicates either that the observed fluxes in the water lines must be extinction corrected with large factors, or more likely, that most of the observed line emission originates at R$\geq$200 pc. This interpretation is consistent with that of Srianand & Petitjean (2000) who find that radiative excitation from a far-IR source larger than the UV source, and at least 200 pc, is required to explain the presence of [SiII] and [CII] in the upper far-IR levels indicated in optical absorption studies.

Without more detailed geometric constraints, we can only conclude that the total mass of water vapor is at least $\sim$50 times that of Mrk 231, some 2.5×10^4 $M_\odot$, and is likely distributed over scales larger than 200 pc, comparable to the 550-pc size-scale inferred from the CO imaging. The mass of water vapor corresponds to an average abundance relative to H_2 of $\geq 1.4 \times 10^{-7}$, when referred to the full molecular gas mass in APM 08279+5255. This estimate is a good match to our our XDR model, which predicts a water abundance of 1.4–2.0×10^{-7} with the parameters described above.

REFERENCES

????

08. 1

Bock, D. C.-J., Bolatto, A. D., Hawkins, D. W., Kemball, A. J., Lamb, J. W., Plambeck, R. L., Pound, M. W., Scott, S. L., Woody, D. P., & Wright, M. C. H. 2006, in Presented at the Society of Photo-Optical Instrumentation Engineers (SPIE) Conference, Vol. 6267, Society of Photo-Optical Instrumentation Engineers (SPIE) Conference Series

Cernicharo, J., Goicoechea, J. R., Daniel, F., Lerate, M. R., Barlow, M. J., Swinyard, B. M., van Dishoeck, E. F., Lim, T. L., Viti, S., & Yates, J. 2006, ApJ, 649, L33

Draine, B. T., & Roberge, W. G. 1982, ApJ, 259, L91

Earle, L., Ade, P., Aguirre, J., Aikin, R., Battle, J., Bock, J., Bradford, C. M., Dragovan, M., Duband, L., Glenn, J., Griffin, G., Hristov, V., Maloney, P., Matsuhara, H., Naylor, B., Nguyen, H., Yun, M., & Zmuidzinas, J. 2006, in SPIE Conference Series, Vol. 6275, Society of Photo-Optical Instrumentation Engineers (SPIE) Conference Series

Ferkinhoff, C., Hailey-Dunsheath, S., Nikola, T., Parshley, S. C., Stacey, G. J., Benford, D. J., & Staguhn, J. G. 2010, ApJ, 714, L147

Fixsen, D. J., Bennett, C. L., & Mather, J. C. 1999, ApJ, 526, 207

González-Alfonso, E., Fischer, J., Isaak, K., Rykala, A., Savini, G., Spaans, M., van der Werf, P., Meijerink, R., Israel, F. P., Loenen, A. F., Vlahakis, C., Smith, H. A., Charmandaris, V., Aalto, S., Henkel, C., Weiß, A., Walter, F., Greve, T. R., Martín-Pintado, J., Naylor, D. A., Spinoglio, L., Veilleux, S., Harris, A. I., Armus, L., Lord, S., Mazzarella, J., Xilouris, E. M., Sanders, D. B., Dasyra, K. M., Wiedner, M. C., Kramer, C., Papadopoulos, P. P., Stacey, G. J., Evans, A. S., & Gao, Y. 2010, A&A, 518, L43+

González-Alfonso, E., Smith, H. A., Ashby, M. L. N., Fischer, J., Spinoglio, L., & Grundy, T. W. 2008, ApJ, 675, 303

Griffin, M. J., Abergel, A., Abreu, A., Ade, P. A. R., André, P., Augueres, J., Babbedge, T., Bae, Y., Baillie, T., Baluteau, J., Barlow, M. J., Bendo, G., Benielli, D., Bock, J. J., Bonhomme, P., Brisbin, D., Brockley-Blatt, C., Caldwell, M., Cara, C., Castro-Rodriguez, N., Cerulli, R., Chanial, P., Chen, S., Clark, E., Clements, D. L., Clerc, L., Coker, J., Communal, D., Conversi, L., Cox, P., Crumb, D., Cunningham, C., Daly, F., Davis, G. R., de Antoni, P., Delderfield, J., Devin, N., di Giorgio, A., Didschuns, I., Dohlen, K., Donati, M., Dowell, A., Dowell, C. D., Duband, L., Dumaye, L., Emery, R. J., Ferlet, M., Ferrand, D., Fontignie, J., Fox, M., Franceschini, A., Frerking, M., Fulton, T., Garcia, J., Gastaud, R., Gear, W. K., Glenn, J., Goizel, A., Griffin, D. K., Grundy, T., Guest, S., Guillemet, L., Hargrave, P. C., Harwit, M., Hastings, P., Hatziminaoglou, E., Herman, M., Hinde, B., Hristov, V., Huang, M., Imhof, P., Isaak, K. J., Israelsson, U., Ivison, R. J., Jennings, D., Kiernan, B., King, K. J., Lange, A. E., Latter, W., Laurent, G., Laurent, P., Leeks, S. J., Lellouch, E., Levenson, L., Li, B., Li, J., Lilienthal, J., Lim, T., Liu, S. J., Lu, N., Madden, S., Mainetti, G., Marliani, P., McKay, D., Mercier, K., Molinari, S., Morris, H., Moseley, H., Mulder, J., Mur, M., Naylor, D. A., Nguyen, H., O'Halloran, B., Oliver, S., Olofsson, G., Olofsson, H., Orfei, R., Page, M. J., Pain, I., Panuzzo, P., Papageorgiou, A., Parks, G., Parr-Burman, P., Pearce, A., Pearson, C., Pérez-Fournon, I., Pinsard, F., Pisano, G., Podosek, J., Pohlen, M., Polehampton, E. T., Pouliquen, D., Rigopoulou, D., Rizzo, D., Roseboom, I. G., Roussel, H., Rowan-Robinson, M., Rownd, B., Saraceno, P., Sauvage, M., Savage, R., Savini, G., Sawyer, E., Scharmberg, C., Schmitt, D., Schneider, N., Schulz, B., Schwartz, A., Shafer, R., Shupe, D. L., Sibthorpe, B., Sidher, S., Smith, A., Smith, A. J., Smith, D., Spencer, L., Stobie, B., Sudiwala, R., Sukhatme, K., Surace, C., Stevens, J. A., Swinyard, B. M., Trichas, M., Tourette, T., Triou, H., Tseng, S., Tucker, C., Turner, A., Vaccari, M., Valtchanov, I., Vigroux, L., Virique, E., Voellmer, G., Walker, H., Ward, R., Waskett, T., Weilert, M., Wesson, R., White, G. J., Whitehouse, N., Wilson, C. D., Winter, B., Woodcraft, A. L., Wright, G. S., Xu, C. K., Zavagno, A., Zemcov, M., Zhang, L., & Zonca, E. 2010, A&A, 518, L3+

Hollenbach, D., & McKee, C. F. 1979, ApJS, 41, 555

Just, D. W., Brandt, W. N., Shemmer, O., Steffen, A. T., Schneider, D. P., Chartas, G., & Garmire, G. P. 2007, ApJ, 665, 1004

Krips, M., Peck, A. B., Sakamoto, K., Petitpas, G. B., Wilner, D. J., Matsushita, S., & Iono, D. 2007, ApJ, 671, L5

Lewis, G. F., Chapman, S. C., Ibata, R. A., Irwin, M. J., & Totten, E. J. 1998, ApJ, 505, L1+

Lupu, R. E., Scott, K. S., Aguirre, J. E., Aretxaga, I., Auld, R., Barton, E., Beelen, A., Bertoldi, F., Bock, J. J., Bonfield, D., Bradford, C. M., Buttiglione, S., Cava, A., Clements, D. L., Cooke, J., Cooray, A., Dannerbauer, H., Dariush, A., De Zotti, G., Dunne, L., Dye, S., Eales, S., Frayer, D., Fritz, J., Glenn, J., Hughes, D. H., Ibar, E., Ivison, R. J., Jarvis, M. J., Kamenetzky, J., Kim, S., Lagache, G., Leeuw, L., Maddox, S., Maloney, P. R., Matsuhara, H., Murphy, E. J., Naylor, B. J., Negrello, M., Nguien, H., Omont, A., Pascale, E., Pohlen, M., Rigby, E., Rodighiero, G., Serjeant, S., Smith, D., Temi, P., Thompson, M., Valtchanov, I., Verma, A., Vieira, J. D., & Zmuidzinas, J. 2010, ArXiv e-prints

Maloney, P. R., Hollenbach, D. J., & Tielens, A. G. G. M. 1996, ApJ, 466, 561

Naylor, B. J., Bradford, C. M., Aguirre, J. E., Bock, J. J., Earle, L., Glenn, J., Inami, H., Kamenetzky, J., Maloney, P. R., Matsuhara, H., Nguyen, H. T., & Zmuidzinas, J. 2010, ApJ, 722, 668

Neufeld, D. A., & Kaufman, M. J. 1993, ApJ, 418, 263

Neufeld, D. A., & Melnick, G. J. 1987, ApJ, 322, 266

Omont, A., Neri, R., Cox, P., Lupu, R., Guélin, M., van der Werf, P., Weiß, A., Ivison, R., Negrello, M., Leeuw, L., Lehnert, M., Smail, I., Verma, A., Baker, A. J., Beelen, A., Aguirre, J. E., Baes, M., Bertoldi, F., Clements, D. L., Cooray, A., Coppin, K., Dannerbauer, H., de Zotti, G., Dye, S., Fiolet, N., Frayer, D., Gavazzi, R., Hughes, D., Jarvis, M., Krips, M., Michałowski, M. J., Murphy, E. J., Riechers, D., Serjeant, S., Swinbank, A. M., Temi, P., Vaccari, M., Vieira, J. D., Auld, R., Buttiglione, B., Cava, A., Dariush, A., Dunne, L., Eales, S. A., Fritz, J., Gomez, H., Ibar, E., Maddox, S., Pascale, E., Pohlen, M., Rigby, E., Smith, D. J. B., Bock, J., Bradford, C. M., Glenn, J., Scott, K. S., & Zmuidzinas, J. 2011, A&A, 530, L3+

Panuzzo, P., Rangwala, N., Rykala, A., Isaak, K. G., Glenn, J., Wilson, C. D., Auld, R., Baes, M., Barlow, M. J., Bendo, G. J., Bock, J. J., Boselli, A., Bradford, M., Buat, V., Castro-Rodríguez, N., Chanial, P., Charlot, S., Ciesla, L., Clements, D. L., Cooray, A., Cormier, D., Cortese, L., Davies, J. I., Dwek, E., Eales, S. A., Elbaz, D., Fulton, T., Galametz, M., Galliano, F., Gear, W. K., Gomez, H. L., Griffin, M., Hony, S., Levenson, L. R., Lu, N., Madden, S., O'Halloran, B., Okumura, K., Oliver, S., Page, M. J., Papageorgiou, A., Parkin, T. J., Pérez-Fournon, I., Pohlen, M., Polehampton, E. T., Rigby, E. E., Roussel, H., Sacchi, N., Sauvage, M., Schulz, B., Schirm, M. R. P., Smith, M. W. L., Spinoglio, L., Stevens, J. A., Srinivasan, S., Symeonidis, M., Swinyard, B., Trichas, M., Vaccari, M., Vigroux, L., Wozniak, H., Wright, G. S., & Zeilinger, W. W. 2010, A&A, 518, L37+

Papadopoulos, P., Ivison, R., Carilli, C., & Lewis, G. 2001, Nature, 409, 58

Rangwala, N., Maloney, P. R., Glenn, J., Wilson, C. D., Rykala, A., Isaak, K., Baes, M., Bendo, G. J., Boselli, A., Bradford, C. M., Clements, D. L., Cooray, A., Fulton, T., Imhof, P., Kamenetzky, J., Madden, S. C., Mentuch, E., Sacchi, N., Sauvage, M., Schirm, M. R. P., Smith, M. W. L., Spinoglio, L., & Wolfire, M. 2011, ArXiv e-prints

Riechers, D. A., Walter, F., Carilli, C. L., & Lewis, G. F. 2009, ApJ, 690, 463

Scoville, N. Z., & Kwan, J. 1976, ApJ, 206, 718

Srianand, R., & Petitjean, P. 2000, A&A, 357, 414

van der Werf, P. P., Isaak, K. G., Meijerink, R., Spaans, M., Rykala, A., Fulton, T., Loenen, A. F., Walter, F., Weiß, A., Armus, L., Fischer, J., Israel, F. P., Harris, A. I., Veilleux, S., Henkel, C., Savini, G., Lord, S., Smith, H. A., González-Alfonso, E., Naylor, D., Aalto, S., Charmandaris, V., Dasyra, K. M., Evans, A., Gao, Y., Greve, T. R., Güsten, R., Kramer, C., Martín-Pintado, J., Mazzarella, J., Papadopoulos, P. P., Sanders, D. B., Spinoglio, L., Stacey, G., Vlahakis, C., Wiedner, M. C., & Xilouris, E. M. 2010, A&A, 518, L42+

Weiß, A., Downes, D., Neri, R., Walter, F., Henkel, C., Wilner, D. J., Wagg, J., & Wiklind, T. 2007, A&A, 467, 955